Trapped Ion Quantum Repeaters with Entanglement Distillation based on Quantum LDPC Codes

Ann Kang
Department of Physics
Carnegie Mellon University
Pittsburgh, PA 15213, USA
annkang@andrew.cmu.edu

Saikat Guha
College of Optical Sciences
University of Arizona
Tucson, AZ 85721, USA
saikat@optics.arizona.edu

Narayanan Rengaswamy
College of Engineering
University of Arizona
Tucson, AZ 85721, USA
narayananr@arizona.edu

Kaushik P. Seshadreesan
School of Computing & Information
University of Pittsburgh
Pittsburgh, PA 15213, USA
kausesh@pitt.edu

2023 IEEE International Conference on Quantum Computing and Engineering (QCE) | 979-8-3503-4323-6/23/$31.00 ©2023 IEEE | DOI: 10.1109/QCE57702.2023.00131

***Abstract*—Quantum repeaters are essential to realizing long-range entanglement distribution networks. To achieve enhanced rates of high-fidelity entanglement distribution, we investigate how entanglement distillation can be used on trapped-ion-based quantum repeater networks. Entanglement distillation is the process of distilling from a large number of copies of low-fidelity entangled qubits a fewer number of copies of higher-fidelity entangled qubits. It has been shown that quantum error-correcting codes (QECCs) can be used to devise protocols for entanglement distillation. In this paper, we consider entanglement distillation based on three lifted-product (LP) quantum low density parity check (QLPDC) codes ([[544, 80, 12]], [[714, 100, 16]], and [[1020, 136, 20]]) on trapped-ion repeater networks with spatial and time multiplexing over various total distances with different inter-repeater spacing to calculate the end-to-end entanglement rates that they enable. The reported rates assume entanglement over each elementary link succeeds synchronously and do not assume any constraint on the number of ions present in each trap. We furthermore assume that distillation occurs at every elementary link and that the entanglement swaps are ideal. Our findings can be considered as groundwork for implementing more efficient distillation and communication protocols on trapped ion networks.**

I. Introduction

In order to realize the full potential of quantum computing, it is essential to inter-connect quantum computers to form quantum networks [1], [2]. Quantum networks that can reliably transfer quantum states and distribute entanglement have been investigated on various qubit platforms, such as superconducting circuits [3], [4], NV centers in diamond [5]–[8], and trapped ions [9], [10]. Protocols for quantum communication across these platforms are being developed and generally involve the use of photons and optical networks [11]–[14]. One significant challenge in developing these optically mediated quantum networks is overcoming a steeply unfavorable rate-loss trade-off [15], [16]. The entanglement distribution capacity between two parties under unlimited rounds of local operations and classical communication (LOCC) is given by $C(\eta) = -\log_2(1-\eta)$ ebits per channel-use [15], where η is the transmissivity of the channel connecting the parties, and an ebit refers to a pair of maximally entangled qubits. When $\eta \ll 1$, $C(\eta) \propto \eta$. Since the transmissivity η of an optical link in long-distance communications decreases exponentially with distance as $e^{-\alpha l}$, with α being the fiber loss coefficient per unit length (typically 0.2 dB/km) and l being the length of the fiber, the entanglement distribution capacity also decays exponentially with distance.

Quantum repeaters have been shown to mitigate the rate-loss trade-off and increase entanglement distribution rates [17]–[20]. In the context of entanglement distribution-based networks, quantum repeaters are specialized quantum processors that establish and store entanglement over smaller distances for which the transmission loss is not as great, and use entanglement swapping to extend the entanglement over longer distances. Trapped-ion systems have become a favored platform for repeater protocols, because they support qubits with long coherence times [21], which is useful for storing entanglement, and optically active ions, which can interface with the network by generating ion-photon entanglement. Trapped-ion systems also support high-fidelity quantum logic gates and exhibit a potential for scalability, making them promising platforms for quantum networking [9].

Repeater architecture based on dual-species trapped ion (DSTI) modules developed by Santra et al. [12] has been shown to exhibit rates that exceed those possible with direct transmission. These dual species modules consist of a communication ion, used to optically herald entanglement, and a memory ion, used to store quantum states for longer times. Already, protocols for DSTI repeater line networks on trapped ion systems with temporal and spatial multiplexing have been investigated to maximize entanglement distribution rates. In our previous work [11], which analyzed a quantum repeater protocol considering ion resources, ion species, number of repeaters, and time and spatial multiplexing, we reported enhanced rates of up to 20000 ebits/second (where an ebit is a maximally entangled qubit pair) at 200km end-to-end distance with repeaters placed every 2km for DSTI modules with $^{138}Ba^{+}$ as communication ions and $^{171}Yb^{+}$ as

KPS thanks NSF grant .

979-8-3503-4323-6/23/$31.00 ©2023 IEEE
DOI 10.1109/QCE57702.2023.00131

Authorized licensed use limited to: University of Arizona. Downloaded on July 24,2024 at 06:22:42 UTC from IEEE Xplore. Restrictions apply.

memory ions and assuming reasonable values for operating parameters. In this work, we investigate how entanglement distillation, the process of distilling from a large number of copies of low-fidelity entangled qubits a fewer number of copies of higher-fidelity entangled qubits, can be incorporated into these repeater protocols to further increase the range of communications, i.e., to distribute entanglement at enhanced rates over larger distances.

In this article, we analyze the rate of successfully performing one round of distillation on every elementary link in a repeater network, which we will also refer to as the end-to-end entanglement rate. We use results from Rengaswamy et al. [22], [23] to obtain the probability of failure of entanglement distillation of Bell pairs with the lifted product (LP) quantum low density parity check (QLDPC) codes, specifically the $[[n, k, d]]$ = [[544, 80, 12]], [[714, 100, 16]], and the [[1020, 136, 20]] codes. We combine these rates with the framework from Dhara et al. [11] to calculate the end-to-end rates using trapped ion repeaters with spatial and time multiplexing. We assume that entanglement is heralded at each elementary link synchronously, entanglement swaps are ideal (meaning that they succeed deterministically and incur no or negligible error in the ebits), successful distillation guarantees that the distilled ebits are of perfect fidelity, there is no constraint on the number of memory and optical ions, and gate operations used in the entanglement distillation are ideal and incur no error. Our results suggest that incorporating entanglement distillation in repeater protocols has the potential to further enhance entanglement distribution rates at farther total end to end distances at rates well above the direct transmission capacity and over repeater schemes that do not employ entanglement distillation.

This article is organized as follows. In section II, we further explain the trapped-ion repeater architecture we consider. In section III, we provide an overview of the quantum error-based entanglement distillation and report the results from Rengaswamy et al. that we use in our rate calculation. In section IV, we present our results for the end-to-end rates with distillation using the LP codes at every elementary link. Finally, in section VI, we present our conclusions.

II. Repeater Architecture and Protocol Outline

The architecture for the trapped ion repeater network that we consider in this article is adopted from Dhara et al. [11], where the repeaters consist of DSTI modules that contain $^{138}Ba^{+}$ ions as the communication ions, and $^{171}Yb^{+}$ ions as the memory ions. These trapped ion repeaters have been shown to enhance entanglement distribution rates beyond the direct transmission capacity. Thus far there are two different types of quantum repeaters, namely, "one-way" quantum error correction and forward transmission based, or "two-way" entanglement distribution and quantum teleportation based, and three distinct generations of quantum repeaters [17]. In this article, we consider two-way 2G quantum repeaters. Two-way repeaters operate by generating distinct ebits over smaller segments of the network which we refer to as elementary links, then use entanglement swaps to extend these local entanglements to eventually be shared between the end parties on the channel. 2G quantum repeaters use heralded entanglement generation and employ quantum error correction. Here we use quantum error correction in two different ways: i) in the form of repetition codes as implemented by spatial and time multiplexed generation of ebits over elementary links, and ii) in the form of codes for entanglement distillation across the elementary links.

For example, consider a network over some total distance L_o, separated into $r+1$ elementary links using r repeaters, where there is a repeater or end node at each end of an elementary link. In two-way quantum repeaters, first, entanglement is established across each elementary link via linear optical Bell state measurements (BSMs) between adjacent repeaters, which has some probability $p \propto \exp(-\alpha L_o/(r+1))$ of succeeding. The clock cycle duration τ of a repeater refers to the rate at which the repeater nodes attempt ion-photon entanglement generation. We assume that all nodes share the same clock cycle. We also assume that the swap operation that transfers entanglement from optical ions to the memory ions via ion-ion gates produces a negligible error.

The use of the repetition code in the form of spatial and time multiplexing helps boost the probability of successfully heralding entanglement along each elementary link [18], [24]–[26]. Spatial multiplexing refers to attempting entanglement $M \in \mathbb{Z}^+$ times in parallel through distinct optical fibers in space. Time multiplexing refers to attempting to herald entanglement $m \in \mathbb{Z}^+$ times over blocks of τ seconds. Time multiplexing does not require multiple physical channels, but achieves the same effect of boosting the heralding rate. In general, the achievable entanglement generation rate with both spatial and time multiplexed two-way repeaters is given as

$$R(L_o, r, m) = \frac{(1-(1-p)^{mM})^{r+1}}{m\tau}. \tag{1}$$

The repeaterless bound on the entanglement generation capacity for multiplexed quantum communications (in ebits/s units), which we will also refer to as the PLOB bound and forms the baseline, is given by:

$$C_{\text{direct}}(\eta, M, \tau) = -\frac{M}{\tau}\log_2(1-\eta) \text{ ebits/s}, \tag{2}$$

Optimizing over M, m, and r, the entanglement generation rate with multiplexed repeaters can beat the PLOB bound.

Here, we investigate if we can further improve the entanglement distribution rates of repeater networks by adding distillation protocols to each elementary link in the network. We consider a distillation step based on the protocol from Rengaswamy et. al [22], [23]. The entanglement distillation is performed on the ebits which were just heralded. We assume that successful distillation produces ebits with perfect fidelity. Then, entanglement swap operations are performed at each node to extend the entanglement over longer distances, which in this paper we assume are ideal and succeed deterministically. Figure 1 shows entanglement distillation

Authorized licensed use limited to: University of Arizona. Downloaded on July 24,2024 at 06:22:42 UTC from IEEE Xplore. Restrictions apply.

across each elementary link followed by an entanglement swap.

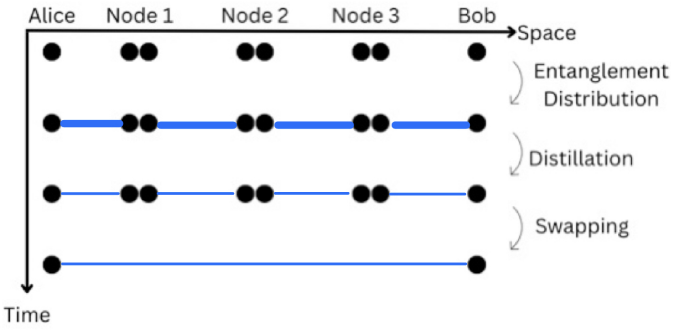

Fig. 1: Entanglement is first heralded between qubits in adjacent nodes (black dots), then are distilled, then swapped. We assume that successful distillation produces ebits with perfect fidelity. The blue lines represent entanglements, where heavier line weight represents a higher number of copies of the entanglement. [27].

Table I summarizes the parameters of our trapped-ion repeater network and their values used in our end-to-end rate calculations.

Parameter	Associated Meaning	Value
τ	Clock cycle duration	0.1μs
τ_g	Ion-ion gate/measurement time	0.1μs
τ_o	Communication ion lifetime	50μs
L_o	Total network distance	variable
M	Degree of spatial multiplexing	10
m	Degree of time multiplexing	variable
η	Transmissivity	0.2dB
η_c	Coupling Collection Efficiency	0.3
η_d	Detection Efficiency	0.8
ϵ_g	Ion-ion gate error rate	0
q	Probability of successful distillation	variable
r	Number of repeaters	variable
$[[n,k,d]]$	Parameters of the QEC code	variable

TABLE I: Timing parameters associated with trapped-ion repeaters.

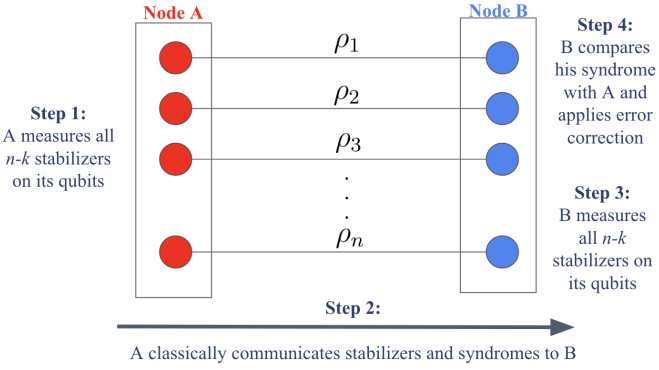

Fig. 2: Nodes A and B use an $[[n,k,d]]$ QEC to distill n Werner pairs. This distillation algorithm is performed on every elementary link between all nodes in our repeater network.

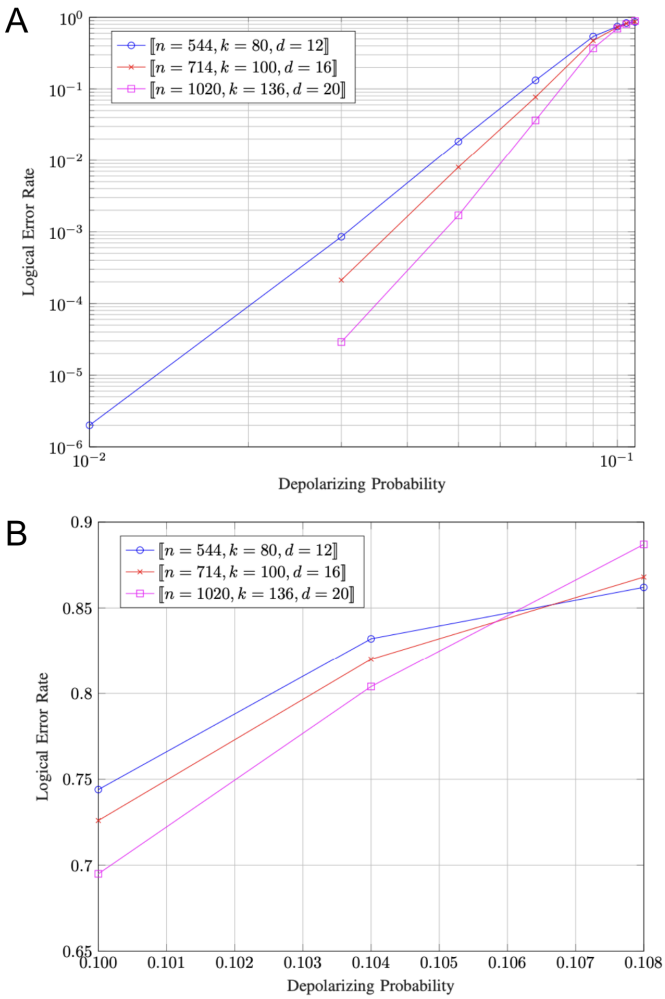

Fig. 3: LP code entanglement distillation simulation results. We interpret the initial fidelity (F_0) of the n Werner pairs as 1-ϵ, where ϵ is the depolarizing probability. Figure A generally suggests that distillation using longer code lengths is more likely to succeed than using shorter code lengths. Figure B is a zoomed-in view of the top right of the graph in Figure A, which reveals a threshold where distillation using the shorter codes outperforms distillation using the longer codes.

The values for L_0 are variable over a range of 30km to 500 km. The time multiplexing parameter m is optimized to maximize the end-to-end rate and thus is also variable. We obtain the probability q that distillation succeeds at one link from Rengaswamy's results and thus calculate the probability of performing successful distillation at all links as q^{r+1}. We consider three different LP codes where $[[n,k,d]] = [[544,80,12]],[[714,100,16]],[[1020,136,20]]$. Note that n also refers to the number of noisy entangled qubit pairs that much be generated initially at each node.

Authorized licensed use limited to: University of Arizona. Downloaded on July 24,2024 at 06:22:42 UTC from IEEE Xplore. Restrictions apply.

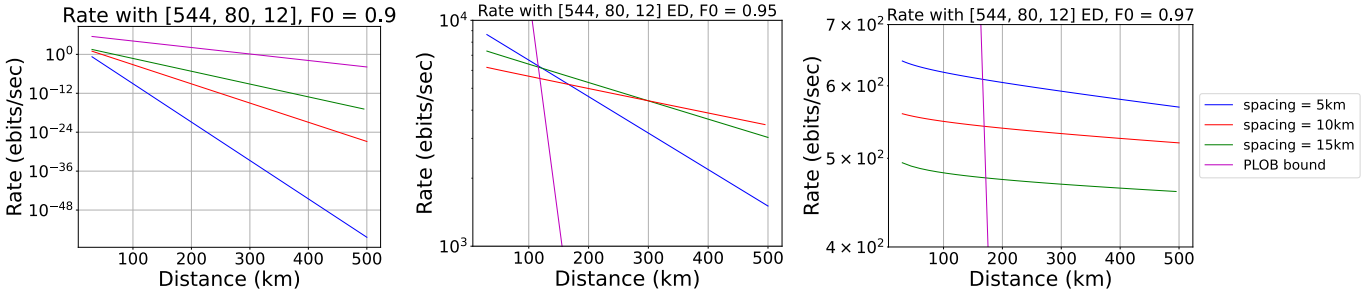

(a) None of the protocols beat the PLOB bound.

(b) All protocols beat the PLOB bound at total distances above 115.75 km.

(c) All protocols beat the PLOB bound at total distances above 166.25 km

Fig. 4: Comparison of rates across different starting fidelities and inter-repeater spacings using the [[544, 80, 12]] code. Distillation performed with higher initial fidelities beat the PLOB bound at larger total distances.

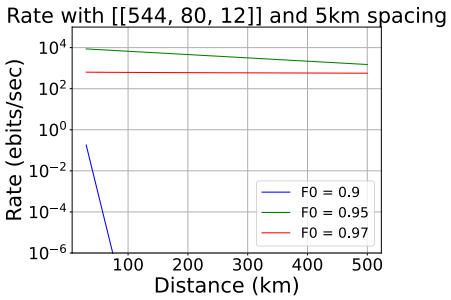

Fig. 5: Comparison of rates across different starting fidelities. The protocol with $F_0 = 0.9$ performs much worse than those with higher fidelities. There appears to be a crossover point where $F_0 = 0.97$ outperforms $F_0 = 0.95$ at higher total distances.

III. Quantum Error Correction Based Entanglement Distillation

Many quantum error correction (QEC) protocols using $[[n, k, d]]$ quantum error correcting codes (QECCs) have been developed to detect and correct coherent errors in quantum states due to external noise [28], [29]. For the purposes of entanglement distillation, we are concerned with the so-called stabilizer codes. An $[[n, k, d]]$ stabilizer code is defined as a commutative subgroup of the Pauli group, $P_n = \{i^\kappa E_1 \otimes E_2 \otimes ... \otimes E_n, E_i \in I, X, Z, Y, \kappa \in \mathbb{Z}_4\}$, that does not contain $-I_n$. We consider the algorithm outlined by Regnaswamy et al. [22], [23] to be used for entanglement distillation at every elementary link of our repeater network. The general steps for distillation between a pair of nodes (let the left node be node A, and the right node be node B) in a network are illustrated in Fig. 2.

It is assumed that all nodes in the network will use a common choice of an $[[n, k, d]]$ QECC to use in the entanglement distillation procedure. Initially, each entangled qubit pair is represented as a Werner state

$$\rho = (1 - \epsilon)\Phi^+ + \frac{\epsilon}{3}(\Phi^- + \Psi^+ + \Psi^-) \tag{3}$$

where $\Phi^+ = |\Phi^+\rangle\langle\Phi^+|$, $\Phi^- = |\Phi^-\rangle\langle\Phi^-|$, $\Phi^+ = |\Psi^+\rangle\langle\Psi^+|$, $\Psi^- = |\Psi^-\rangle\langle\Phi^-|$ are the maximally entangled Bell state density operators, where $|\Phi^\pm\rangle = (|0,1\rangle \pm |1,0\rangle)/2$ and $|\Psi^\pm\rangle = (|0,0\rangle \pm |1,1\rangle)/2$ represent the maximally entangled Bell states in the computational Z basis. The Werner state accounts for possible errors from noise that may be present in the initial states and the probabilistic nature of the entanglement generation if the generation is unheralded. $F_0 = 1 - \epsilon$, where ϵ is some depolarizing probability, is defined as the fidelity of the entangled state.

Node A and node B each begin with one qubit from each of n Werner pairs. Node A first measures each of its $n - k$ code stabilizers on its n qubits and obtains a syndrome for each measurement. The syndromes and the stabilizers are sent to node B over a noiseless classical channel. Node B then also measures those stabilizer generators on its n qubits, and obtains its own syndromes. The results with the information of Node A's syndromes are used to determine whether corrections of any Pauli errors need to be performed. After performing any necessary corrections, the procedure produces k pairs of logical qubits if the channel error was correctable. Otherwise there is still some unknown error on the final k qubits. More detail on this algorithm can be found in Ref. [30]. The $[[n, k, d]]$ codes that we chose for the entanglement distillation are the $[[544, 80, 12]]$, $[[714, 100, 16]]$, and the [[1020, 136, 20]] LP QLPDC codes, a type of CSS code. QLDPC codes are block codes that have a parity check matrix H in which every row and column of H is "sparse". The advantages of QLDPC codes are that the syndromes can be measured with sparse interactions (only order n interactions instead of n^2) and they support practical decoding algorithms. Also, QLDPC codes are flexible; it is possible to construct them for arbitrary rates, lengths, and code distances. They are also good codes in the sense that the code distance scales linearly with the length of the code. For more detail on the construction and definition of QLDPC codes, refer to [31]–[35].

We use the results from Rengaswamy et al. to obtain the probability of success of the distillation on entangled bell pairs for the $[[544, 80, 12]]$, $[[714, 100, 16]]$, and the

Authorized licensed use limited to: University of Arizona. Downloaded on July 24,2024 at 06:22:42 UTC from IEEE Xplore. Restrictions apply.

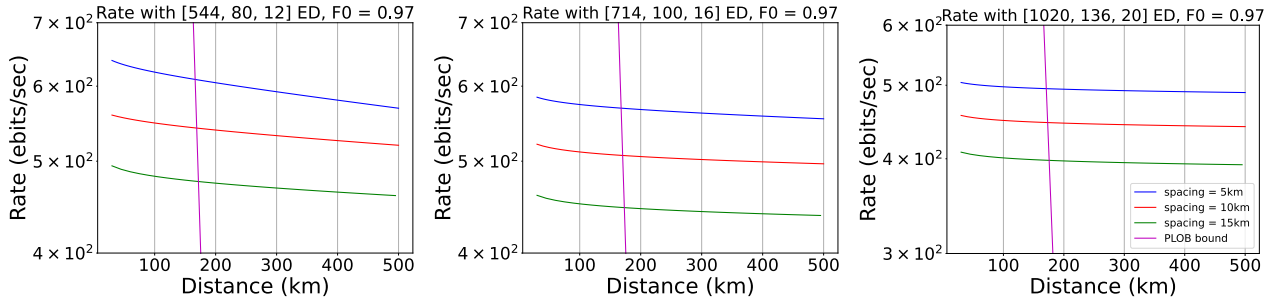

(a) All protocols beat the PLOB bound at total distances above 166.25 km.

(b) All protocols beat the PLOB bound at total distances above 167.5 km.

(c) All protocols beat the PLOB bound at total distances above 171 km

Fig. 6: Comparison of rates across different choice of QECC used for distillation with starting fidelity of 0.97. The protocols employing larger QECCs beat the PLOB bound at greater distances.

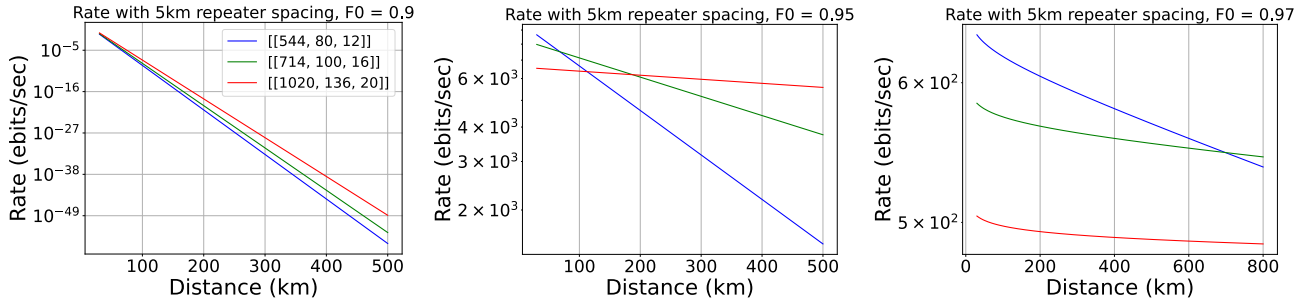

(a) The protocol with the larger code produces better rates than smaller code families.

(b) At distances above 187.4 km, the 1020 code protocol produces the best rates.

(c) Extending these curves, there appears to be similar thresholding behavior where at larger distances, the 1020 protocol outperforms the others.

Fig. 7: Comparison of rates across different code lengths and different initial starting fidelities. The protocols with higher fidelities $F_0 = 0.95$ and $F_0 = 0.97$ exhibit a threshold below which the 544 code performs the best and above which the 1020 code performs the best. This threshold appears to increase as F_0 increases.

$[[1020, 136, 20]]$ LP codes. Figure 3 shows the logical error rate for these codes, which we take as the probability that the distillation based on the codes fails, for various depolarizing probability values (ϵ). Here we take the initial fidelity F_0 of the entangled bell pairs as $1 - \epsilon$. The results show how longer codes generally have lower failure probability and how higher initial fidelity yields lower failure probability.

IV. Results

Our results show how factors such as inter-repeater spacing, initial fidelity (F_0), and code family (either the [[544, 80, 12]], [[714, 100, 16]], and [[1020, 136, 20]] impact the end-to-end rate at different total distances L_0, where the end-to-end rate refers to the probability of successfully performing distillation on every elementary link in the network.

Figure 4 shows how the initial fidelity of the bell pairs affects the rates, as well as the threshold distance where the distillation protocol beats the PLOB bound. We observe that for initial fidelity of 0.9 and choice of code of [[544, 80, 12]], none of the repeater protocols beat the PLOB bound. We also notice that for lower fidelities, the repeater protocol beats the PLOB bound at a lower distance. The plots in figure 4 are also generally representative of the behavior for the higher codes [[714, 100, 16]] and [[1020, 136, 20]], with the exception that the protocol with $F_0 = 0.9$ for both of the higher codes will beat the PLOB bound. For both of the higher codes, we similarly notice that lower fidelities beat the PLOB bound at lower distances.

Figure 5 shows a better visualization of how the initial fidelities change the end-to-end rate for the [[544, 80, 12]] code. We observe that the protocol with $F_0 = 0.9$ has the worst rate which declines exponentially with distance. $F_0 = 0.95$ and $F_0 = 0.97$ exhibit higher rates that remain almost constant over distance. The rate for $F_0 = 0.97$, the higher fidelity, is worse than the rate for $F_0 = 0.95$. Figure 5 is representative of the behavior for the higher codes as well, as they exhibit the same relationship between F_0 and end-to-end rate; the rates for protocols with $F_0 = 0.9$ decay exponentially with distance, while the rates for protocols with $F_0 = 0.95$ and $F_0 = 0.97$ remain almost constant, with the rates for $F_0 = 0.95$ being slightly better than those for $F_0 = 0.97$.

Figure 6 shows how the choice of code family impacts

Authorized licensed use limited to: University of Arizona. Downloaded on July 24,2024 at 06:22:42 UTC from IEEE Xplore. Restrictions apply.

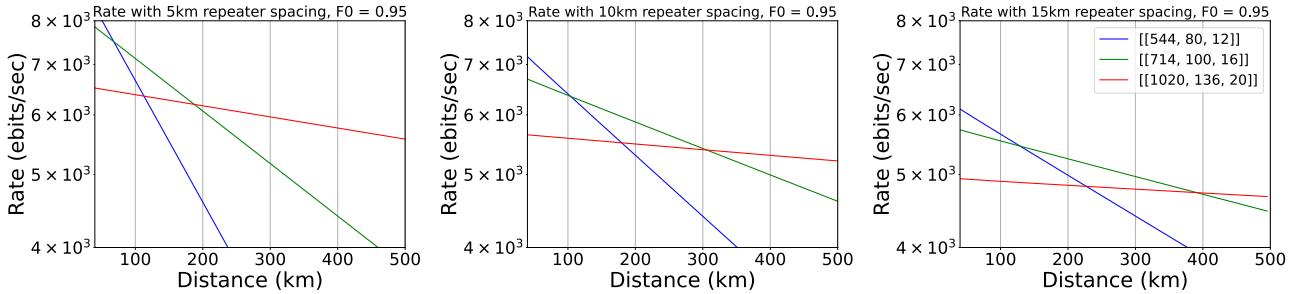

(a) At distances above 187.4 km, the 1020 code produces the best results.

(b) At distances above 305 km, the 1020 code produces the best results.

(c) At distances above 391.7 km, the 1020 code produces the best results.

Fig. 8: Comparison of rates across different inter-repeater spacing. Increasing the inter-repeater spacing worsens the overall rate for each protocol. It also increases the threshold at which the longer 1020 code outperforms the shorter codes.

end-to-end rate for fixed fidelity and the threshold distance at which the repeater protocols beat the PLOB bound. We observe generally that lower code families beat the PLOB bound at lower distances. We also note how generally the smaller codes have higher rates for the same distances, and how larger inter-repeater spacing also worsens the rate. Figure 6 is representative of the behavior fixed at the other fidelities $F_0 = 0.9$ and $F_0 = 0.95$.

Figure 7 is a better visualization showing how the choice in code family for fixed inter-repeater spacing and fidelity impacts the overall rate. For protocols with $F_0 = 0.9$, the largest code, [[1020, 136, 20]] yields the best rates, while the smallest code, [[544, 80, 12]] performs the worst. For $F_0 = 0.95$ and $F_0 = 0.97$, there appears to be a threshold. For distances underneath this threshold, the largest code has the worst rates, and the smallest code has the best rates. But above the threshold, the behavior reverses and the largest code performs the best, similar to the behavior for the protocol for $F_0 = 0.9$. For $F_0 = 0.97$, this threshold appears to be beyond $L_0 = 500$ km. The plots in Figure 7 are also representative of the behavior for the other inter-repeater spacings as well.

Figure 8 demonstrates how the inter-repeater spacing impacts the rate and threshold where the protocols with different codes beat each other. Increasing the inter-repeater spacing appears to worsen the rates for all repeater protocols; this relationship is consistent also with the trend in Figure 6. Increasing the inter-repeater spacing also increases the threshold at which the larger codes beat the shorter ones. The protocols for $F_0 = 0.9$ do not exhibit any thresholding behavior; the largest code has strictly better rates for all inter-repeater spacings similar to the behavior shown in Figure 7A.

V. Conclusions

In general, we found interesting relationships between factors such as inter-repeater spacing, choice of QEC, initial fidelity and end-to-end rate for entanglement distillation enabled trapped ion repeaters. All protocols beat the PLOB at some threshold distance except for the protocols with the [[544, 80, 12]] code at elementary link fidelity $F_0 = 0.9$ (Fig. 4). This is probably due to the lower probability of success of distillation of the small [[544, 80, 12]] code and low initial fidelity. From Rengaswamy et al. [22]'s results, we see that distillation with higher codes on ebits with higher initial fidelity is more likely to succeed. Increasing initial fidelity (holding code and spacing constant) improves the rate. The protocols with $F_0 = 0.9$ have the worst rate which decreases exponentially with distance. Again, this can probably be attributed to the fact that lower initial fidelity exponentially deteriorates the probability of success of the distillation. Protocols with $F_0 = 0.95$ have the best rate which is almost constant with distance. Protocols with $F_0 = 0.97$ exhibit slightly worse rates than those with $F_0 = 0.95$, but also remain almost constant with increasing L_0. The threshold where the repeater protocols beat the PLOB bound also increases with increasing initial fidelity (Figs. 4 and 5). Increasing the QEC code length (holding spacing and fidelity constant) increases the threshold where the repeater protocol beats the PLOB bound (Fig. 6). Increasing code length (holding spacing and fidelity constant) affects the end-to-end rates as well. For protocols with $F_0 = 0.9$, longer codes perform strictly better. For the higher fidelities, a threshold appears; for protocols with $F_0 = 0.95$, below the threshold at short distances, shorter codes perform better but at long distances, longer codes perform better. For protocols with $F_0 = 0.97$, there appears to be similar thresholding behavior at distances beyond 500 km (Fig. 7). Increasing the inter-repeater spacing (holding code and fidelity constant), worsens the end-to-end rate. The results in Figs. 6 and 9 show that lower inter-repeater spacings have better rates. Increasing the inter-repeater spacing also increases the threshold where higher codes beat lower codes as shown in Fig. 8. Future work may include asynchronous cases, where success elementary links are stored beyond a time block in the long lifetime trapped ion qubits, considering ion number requirements, considering distillation not on every elementary link, considering iterative distillation, and considering end-to-end distillation.

References

[1] S. Wehner, D. Elkouss, and R. Hanson, "Quantum internet: A vision for the road ahead," Science, vol. 362, Oct. 2018.

Authorized licensed use limited to: University of Arizona. Downloaded on July 24,2024 at 06:22:42 UTC from IEEE Xplore. Restrictions apply.

[2] R. Van Meter, Quantum Networking. John Wiley & Sons, May 2014.

[3] H. Yan, Y. Zhong, H.-S. Chang, A. Bienfait, M.-H. Chou, C. R. Conner, É. Dumur, J. Grebel, R. G. Povey, and A. N. Cleland, "Entanglement purification and protection in a superconducting quantum network," Phys. Rev. Lett., vol. 128, p. 080504, Feb. 2022.

[4] Z.-Q. Yin, W. L. Yang, L. Sun, and L. M. Duan, "Quantum network of superconducting qubits through an optomechanical interface," Phys. Rev. A, vol. 91, p. 012333, Jan. 2015.

[5] M. Pompili, S. L. N. Hermans, S. Baier, H. K. C. Beukers, P. C. Humphreys, R. N. Schouten, R. F. L. Vermeulen, M. J. Tiggelman, L. Dos Santos Martins, B. Dirkse, S. Wehner, and R. Hanson, "Realization of a multinode quantum network of remote solid-state qubits," Science, vol. 372, pp. 259–264, Apr. 2021.

[6] N. Kalb, A. A. Reiserer, P. C. Humphreys, J. J. W. Bakermans, S. J. Kamerling, N. H. Nickerson, S. C. Benjamin, D. J. Twitchen, M. Markham, and R. Hanson, "Entanglement distillation between solid-state quantum network nodes," Science, vol. 356, pp. 928–932, June 2017.

[7] K. Nemoto, M. Trupke, S. J. Devitt, B. Scharfenberger, K. Buczak, J. Schmiedmayer, and W. J. Munro, "Photonic quantum networks formed from NVâ centers," Sci. Rep., vol. 6, p. 26284, May 2016.

[8] L. Childress and R. Hanson, "Diamond NV centers for quantum computing and quantum networks," MRS Bull., vol. 38, pp. 134–138, Feb. 2013.

[9] L. J. Stephenson, D. P. Nadlinger, B. C. Nichol, S. An, P. Drmota, T. G. Ballance, K. Thirumalai, J. F. Goodwin, D. M. Lucas, and C. J. Ballance, "High-Rate, High-Fidelity entanglement of qubits across an elementary quantum network," Phys. Rev. Lett., vol. 124, p. 110501, Mar. 2020.

[10] L.-M. Duan and C. Monroe, "Colloquium: Quantum networks with trapped ions," Rev. Mod. Phys., vol. 82, pp. 1209–1224, Apr. 2010.

[11] P. Dhara, N. M. Linke, E. Waks, S. Guha, and K. P. Seshadreesan, "Multiplexed quantum repeaters based on dual-species trapped-ion systems," Phys. Rev. A, vol. 105, p. 022623, Feb. 2022.

[12] S. Santra, S. Muralidharan, M. Lichtman, L. Jiang, C. Monroe, and V. S. Malinovsky, "Quantum repeaters based on two species trapped ions," New J. Phys., vol. 21, p. 073002, July 2019.

[13] I. V. Inlek, C. Crocker, M. Lichtman, K. Sosnova, and C. Monroe, "Multispecies Trapped-Ion node for quantum networking," Phys. Rev. Lett., vol. 118, p. 250502, June 2017.

[14] L.-M. Duan, B. B. Blinov, D. L. Moehring, and C. Monroe, "Scalable trapped ion quantum computation with a probabilistic Ion-Photon mapping," Jan. 2004.

[15] S. Pirandola, R. Laurenza, C. Ottaviani, and L. Banchi, "Fundamental limits of repeaterless quantum communications," Nat. Commun., vol. 8, p. 15043, Apr. 2017.

[16] M. Takeoka, S. Guha, and M. M. Wilde, "Fundamental rate-loss tradeoff for optical quantum key distribution," Nat. Commun., vol. 5, p. 5235, Oct. 2014.

[17] S. Muralidharan, L. Li, J. Kim, N. Lütkenhaus, M. D. Lukin, and L. Jiang, "Optimal architectures for long distance quantum communication," Sci. Rep., vol. 6, p. 20463, Feb. 2016.

[18] S. Guha, H. Krovi, C. A. Fuchs, Z. Dutton, J. A. Slater, C. Simon, and W. Tittel, "Rate-loss analysis of an efficient quantum repeater architecture," Phys. Rev. A, vol. 92, p. 022357, Aug. 2015.

[19] W. J. Munro, K. Azuma, K. Tamaki, and K. Nemoto, "Inside quantum repeaters," IEEE J. Sel. Top. Quantum Electron., vol. 21, pp. 78–90, May 2015.

[20] H.-J. Briegel, W. Dür, J. I. Cirac, and P. Zoller, "Quantum repeaters: The role of imperfect local operations in quantum communication," Phys. Rev. Lett., vol. 81, pp. 5932–5935, Dec. 1998.

[21] Y. Wang, M. Um, J. Zhang, S. An, M. Lyu, J.-N. Zhang, L.-M. Duan, D. Yum, and K. Kim, "Single-qubit quantum memory exceeding ten-minute coherence time," Nat. Photonics, vol. 11, pp. 646–650, Sept. 2017.

[22] N. Rengaswamy, N. Raveendran, A. Raina, and B. Vasić, "Entanglement purification with quantum LDPC codes and iterative decoding," Oct. 2022.

[23] N. Rengaswamy, A. Raina, N. Raveendran, and B. Vasić, "Distilling GHZ states using stabilizer codes," Sept. 2021.

[24] P. Dhara, A. Patil, H. Krovi, and S. Guha, "Subexponential rate versus distance with time-multiplexed quantum repeaters," Phys. Rev. A, vol. 104, p. 052612, Nov. 2021.

[25] K. P. Seshadreesan, H. Krovi, and S. Guha, "Continuous-variable quantum repeater based on quantum scissors and mode multiplexing," Phys. Rev. Research, vol. 2, p. 013310, Mar. 2020.

[26] H. Krovi, S. Guha, Z. Dutton, J. A. Slater, C. Simon, and W. Tittel, "Practical quantum repeaters with parametric down-conversion sources," Appl. Phys. B, vol. 122, Mar. 2016.

[27] F. Furrer and W. J. Munro, "Repeaters for continuous-variable quantum communication," Phys. Rev. A, vol. 98, p. 032335, Sept. 2018.

[28] J. Roffe, "Quantum error correction: an introductory guide," Contemporary Physics, vol. 60, pp. 226–245, July 2019.

[29] S. J. Devitt, W. J. Munro, and K. Nemoto, "Quantum error correction for beginners," Rep. Prog. Phys., vol. 76, p. 076001, July 2013.

[30] N. Raveendran, N. Rengaswamy, A. K. Pradhan, and B. Vasić, "Soft syndrome decoding of quantum LDPC codes for joint correction of data and syndrome errors," in 2022 IEEE International Conference on Quantum Computing and Engineering (QCE), pp. 275–281, Sept. 2022.

[31] N. P. Breuckmann and J. N. Eberhardt, "Quantum Low-Density Parity-Check codes," PRX Quantum, vol. 2, p. 040101, Oct. 2021.

[32] N. P. Breuckmann and J. N. Eberhardt, "Balanced product quantum codes," IEEE Trans. Inf. Theory, vol. 67, pp. 6653–6674, Oct. 2021.

[33] P. Panteleev and G. Kalachev, "Quantum LDPC codes with almost linear minimum distance," IEEE Trans. Inf. Theory, vol. 68, pp. 213–229, Jan. 2022.

[34] A. Leverrier and G. Zémor, "Quantum tanner codes," in 2022 IEEE 63rd Annual Symposium on Foundations of Computer Science (FOCS), pp. 872–883, Oct. 2022.

[35] M. B. Hastings, J. Haah, and R. O'Donnell, "Fiber bundle codes: breaking the n1/2 polylog(n) barrier for quantum LDPC codes," in Proceedings of the 53rd Annual ACM SIGACT Symposium on Theory of Computing, STOC 2021, (New York, NY, USA), pp. 1276–1288, Association for Computing Machinery, June 2021.

Authorized licensed use limited to: University of Arizona. Downloaded on July 24,2024 at 06:22:42 UTC from IEEE Xplore. Restrictions apply.